

Electronic Supplementary Information

Columnar liquid-crystalline J-aggregates based on N-core-substituted naphthalene diimides

Eduardo Castellanos,^a Rosa María Gomila,^a Rasitha Manha Veedu,^b Gustavo Fernández,^b Antonio Frontera,^{*a} Bartolomé Soberats^{*a}

^a Department of Chemistry, University of the Balearic Islands, Cra. Valldemossa, Km. 7.5, Palma de Mallorca, Spain

^b Organisch-Chemisches Institut Westfälische Wilhelms, Universität Münster, Corrensstraße 36, 48149 Münster, Germany

Table of Contents

- 1. Experimental methods**
- 2. Synthetic procedures**
- 3. NMR Spectra**
- 4. Fluorescence studies in solution**
- 5. UV/Vis experiments in solution**
- 6. Morphology studies of the supramolecular polymers**
- 7. DSC experiments**
- 8. X-ray studies**
- 9. Polarized experiments for NDI-1**
- 10. Transition dipole moment for NDI-1**
- 11. Fourier transform infrared spectroscopy studies**
- 12. Molecular modelling**
- 13. Mechanochromic experiments**
- 14. References**

1. Experimental methods

NMR: NMR spectra were recorded on an Advance (300 MHz) from Bruker at 295 K. The spectra were calibrated using the residual protic solvent as internal standard and the chemical shifts (δ) are recorded in parts per million (ppm).

Mass spectrometry: ESI-HRMS mass spectra were measured on Thermo Scientific Orbitrap Q Exactive mass spectrometer equipped with electrospray modules.

UV/ Vis Spectroscopy: The measurements in solution were carried out with Jasco V-750 UV-vis spectrometer in quartz glass cuvettes (Hellma) using spectroscopic grade chloroform (99%+ stabilized with amylene) and methylcyclohexane (99%) from ACROS. The solid-state experiments were measured with Agilent Cary 5000 UV-Vis-NIR equipped with Diffuse Reflectance accessory (DRA-2500) using 1.25 mm quartz round plates (Hellma).

AFM: Atomic force microscopy images were taken with a Veeco NanoScope IV MultiMode (Veeco, Santa Barbara, CA) using tapping mode.

Infrared: Fourier transform infrared-attenuated total reflection (FTIR-ATR) spectra were recorded on a Bruker Tensor 27 equipped with a PLATINUM Diamond ATR accessory. The spectra were recorded over a range of 400–4000 cm^{-1} and an average of 16 scans was taken for each spectrum.

Fluorescence spectroscopy: Fluorescence excitation-emission spectra were recorded on a Cary Eclipse spectrophotometer. The measurements were carried out in quartz glass cuvettes (Hellma) using spectroscopic grade chloroform (99%+ stabilized with amylene) and methyl cyclohexane (99%) from ACROS. Slit widths were set to 5 mm bandpass for both excitation and emission. All spectra were recorded at 25 ± 1 °C.

X-ray scattering: Middle angle X-ray scattering measurements were performed on a XENOCS XEUSS 3.0. The instrument is equipped with a GeniX 3D Cu micro focus X-ray source ($\lambda = 1.54$ Å; flux = 2×10^8 ph/s) and a DECTRIS Pilatus3 R 300K silicon pixel detector with 487×619 pixels of 172×172 μm in size. All the samples were measured in 1.5 mm glass capillaries (WJM, Germany). The distance sample-detector was calibrated using silver behenate standard sample.

DSC: Differential scanning calorimetry measurements were carried out with a Mettler Toledo DSC 3+. The data given for the thermal transitions were obtained from the second heating and first cooling scans.

POM: Polarizing optical microscopy images were obtained with a Leica DM2700P microscope equipped with Flexacam and a Linkam LTS420 heating stage stage.

Confocal Microscope: Leica SPE, using 100x oil immersion objective. Samples were excited using 532 nm laser, and emission collected at two different “wavelength windows”: 610-630 nm (green) and 650-680 nm (red). Images were processed using LAS-X software. For sample preparation, the solution of NDI-2 ($c = 5 \times 10^{-4}$ M) in MCH was drop-casted on a glass plate and measured after drying of the sample at open air.

2. Synthetic procedures

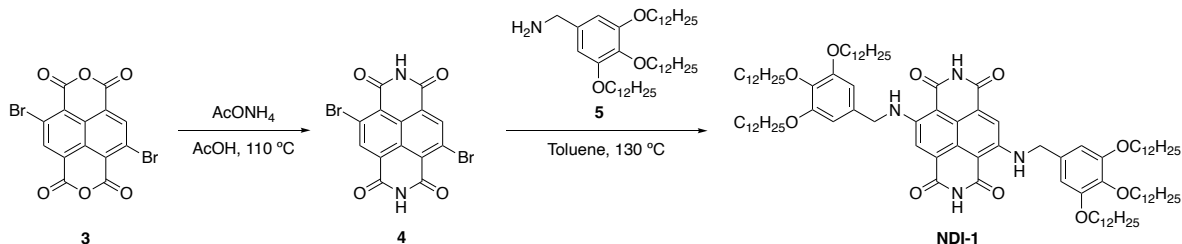


Fig. S1. Synthetic scheme of **NDI-1**.

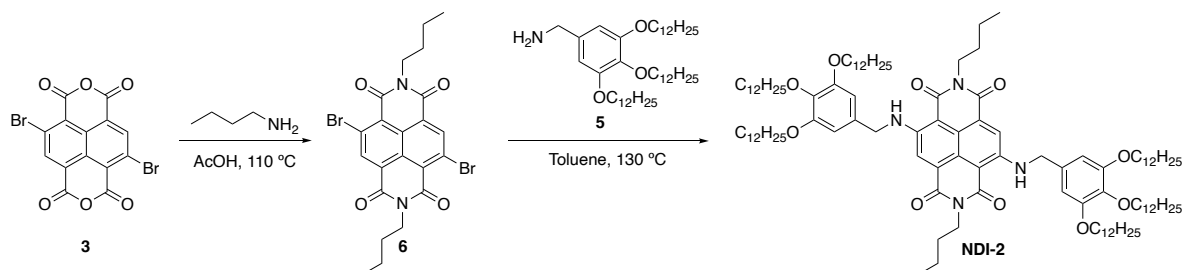


Fig. S2. Synthetic scheme of **NDI-2**.

Compounds **4** and **6** were synthesized according with references S1 and S2, respectively. Compound **5** was prepared according to reference S3.

Compound 4

Compound **3** (300 mg, 0.7 mmol) and ammonium acetate (1.1 g, 14.0 mmol) were dissolved in glacial acetic acid (15 mL). The mixture was refluxed under argon atmosphere overnight. The precipitate obtained was filtered, washed with copious amounts of DI water and dried over vacuum to obtain 0.25 g of yellow solid (84%). The NMR spectrum matched with the previously reported,^{S1} and the compound was used directly in the next step.

¹H-NMR (300 MHz, DMSO-*d*⁶) δ (ppm): 8.62 (ArH, 2H), 12.24 (-NH, 2H).

Compound 6

Compound **3** (100 mg, 0.23 mmol) and n-butyl amine (100 mL, 1 mmol) were dissolved in glacial acetic acid (10 mL). The mixture was refluxed under argon atmosphere overnight. The precipitate obtained was filtered, washed with copious amounts of DI water and dried over vacuum to obtain 120 mg of orange solid (95%). The NMR spectrum matched with the previously reported,^{S2} and the compound was used directly in the next step.

¹H-NMR (300 MHz, CDCl₃) δ (ppm): 0.99 (-CH₃, 6H), 1.25 (-CH₂-, 4H), 1.73 (-CH₂-, 4H), 4.20 (N-CH₂-, 4H), 9.00 (ArH, 2H).

Naphthalene diimide 1

Compound **4** (311 mg, 0.47 mmol) and compound **5^{S3}** (50 mg, 0.12 mmol) were dispersed in 15 mL of dry toluene and refluxed 48h under argon atmosphere. The solvent was removed under low pressure and the crude was purified with column chromatography using dichloromethane:hexane mixture (8:2) as eluent. The product were precipitated in dichlorometane:acetone to obtaing 150 mg of a blue solid (70%).
¹H-NMR (300 MHz, CDCl₃) δ (ppm): 0.88 (-CH₃, 18H), 1.25 (-CH₂-, 96H), 1.44-1.47 (-CH₂-, 12H), 1.75 (-CH₂-, 12H), 3.95 (-OCH₂-, 12H), 4.61 (Ar-CH₂-, 4H), 6.58 (ArH, 4H), 8.19 (ArH(NDI), 2H), 8.33 (-NH-, 2H), 9.53 (NH (NDI), 2H).

¹³C-NMR (75 MHz, 298 K, CDCl₃) δ (ppm): 166.03, 162.56, 153.77, 149.35, 138.00, 132.32, 126.68, 123.25, 118.85, 106.02, 102.43, 73.63, 69.40, 47.67, 32.12, 30.54, 29.96-29.57, 26.3, 22.89, 14.31.

FTIR (ATR, 298 K) ν (cm⁻¹): 3300, 3150, 3020, 2943, 2918, 2850, 1730, 1660, 1580, 1490, 1460, 1435, 1372, 1318, 1248, 1119, 1014, 911, 865, 788, 758, 730, 709, 686, 643, 580, 536, 519, 466.

HRMS ESI (+) for C₁₀₀H₁₆₄N₄O₁₀ [MH]⁺_{calc} = 1582,25 g/mol; [MH]⁺_{exp} = 1582,31 g/mol.

Melting Point (DSC): 158 °C.

Naphthalene diimide 2

Compound **6** (125 mg, 0.20 mmol) and compound **5^{S3}** (25 mg, 0.05 mmol) were dispersed in 10 mL of dry toluene and refluxed 48h under argon atmosphere. The solvent was removed under low pressure and the crude was purified with column chromatography using ethyl acetate:hexane mixture (2:8) as eluent. The product were precipitated in dichlorometane:acetone to obtaing 45 mg of a blue solid (53%)
¹H-NMR (300 MHz, CDCl₃) δ (ppm): 0.83 (-CH₃, 18H), 0.98 (-CH₃, 6H), 1.25 (-CH₂-, 96H) 1.43-1.45 (-CH₂-, 16H), 1.71-1.82 (-CH₂-, 16H), 3.90-3.99 (-O-CH₂-, 12H), 4.13-4.18 (Ar-CH₂-, 4H), 4.59-4.61 (N-CH₂-, 4H), 6.60 (ArH, 4H), 8.21 (ArH(NDI), 2H), 9.71 (-NH-, 2H).

¹³C-NMR (75 MHz, 298 K, CDCl₃) δ (ppm): 166.85, 164.95, 153.06, 144.56, 135.01, 124.42, 121.90, 110.02, 105.59, 102.04, 94.69, 90.41, 70.38, 69.27, 68.76, 61.33, 47.57, 39.35, 37.09, 31.47, 29.31-28.91, 25.66, 22.23, 19.98, 13.65, 12.38.

FTIR (ATR, 298 K) ν (cm⁻¹): 3294, 2945, 2903, 2835, 1702, 1682, 1614, 1566, 1498, 1456, 1425, 1378, 1340, 1303, 1227, 1195, 1152, 1136, 1107, 1052, 1013, 978, 937, 897, 873, 829, 807, 777, 745, 705, 659, 631, 603, 569, 538, 507, 449, 420.

HRMS ESI (+) for C₁₀₀H₁₆₄N₄O₁₀ [MH]⁺_{calc} = 1694.37 g/mol; [MH]⁺_{exp} = 1694.39 g/mol

Melting Point (DSC): 70 °C.

3. NMR Spectra

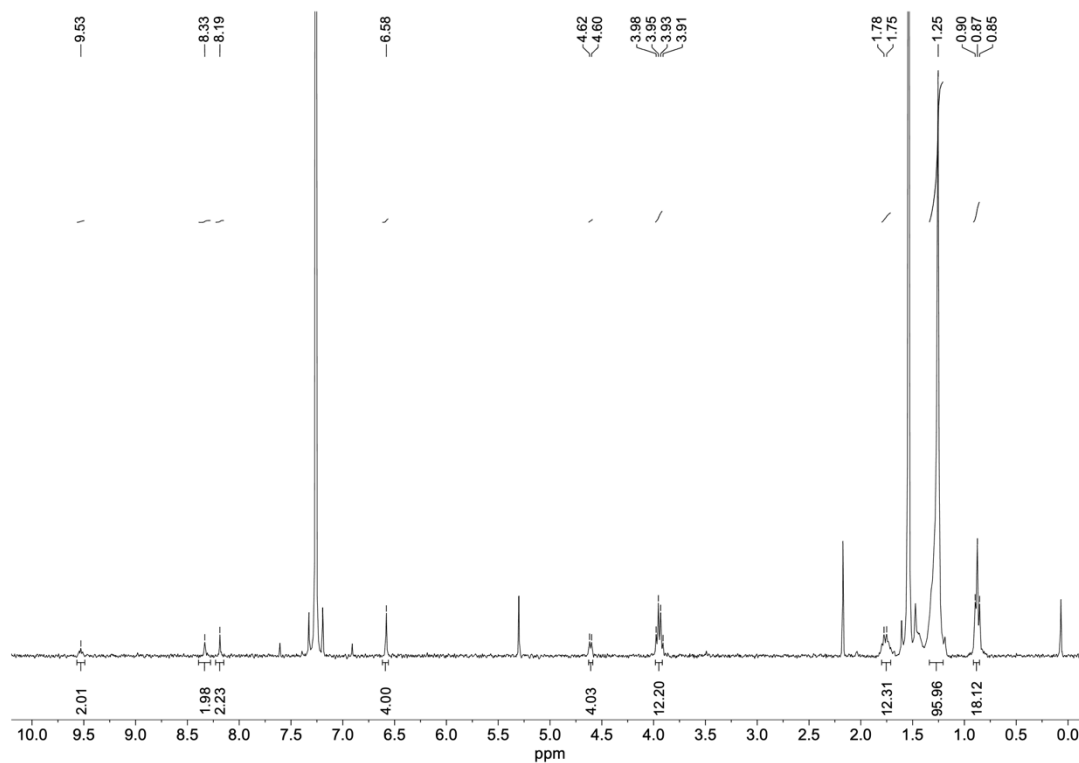


Fig. S3. ^1H -NMR spectrum of NDI-1 in CDCl_3 .

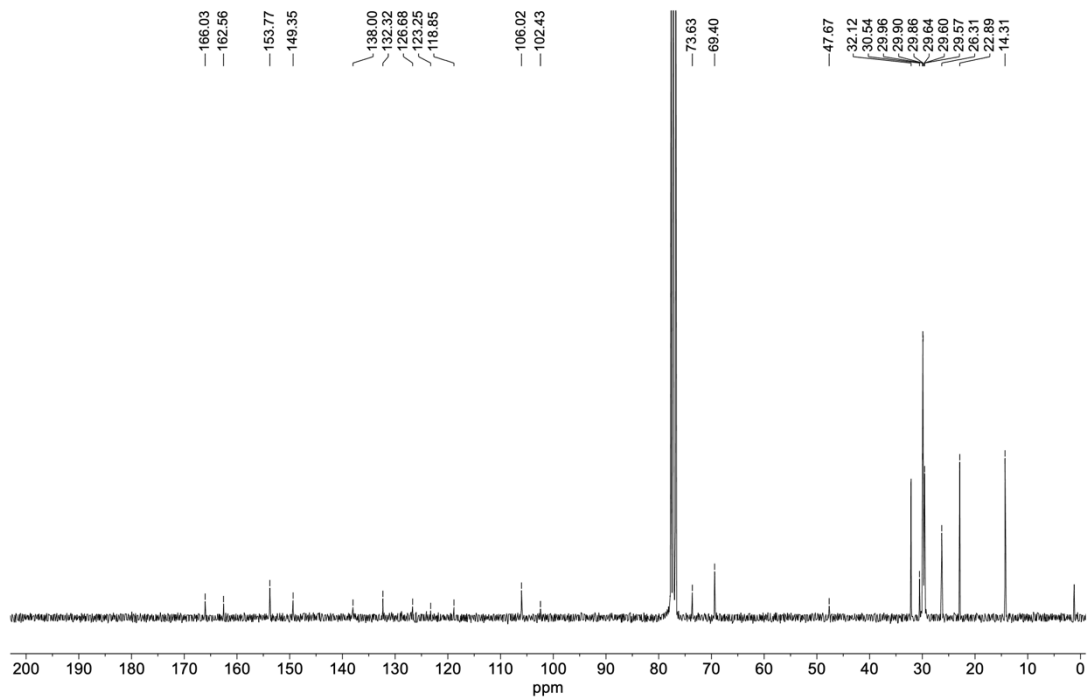


Fig. S4. ^{13}C -NMR spectrum of NDI-1 in CDCl_3 .

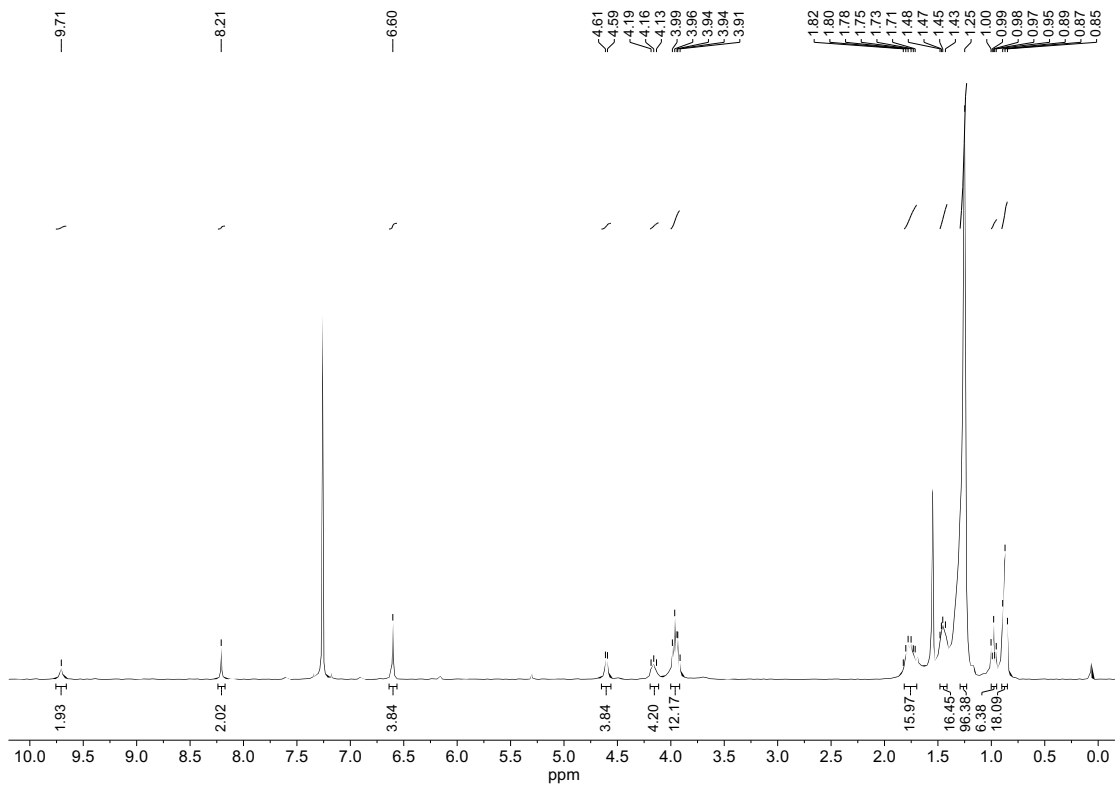


Fig. S5. $^1\text{H-NMR}$ spectrum of NDI-2 in CDCl_3 .

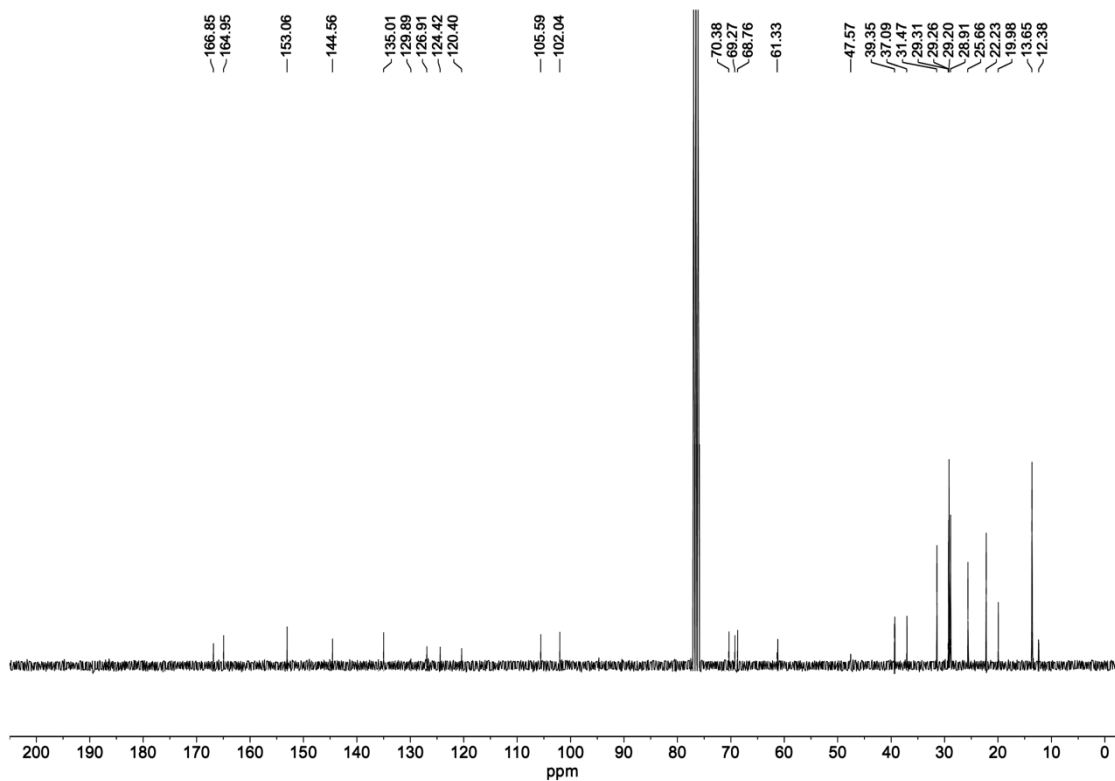


Fig. S6. $^{13}\text{C-NMR}$ spectrum of NDI-2 in CDCl_3 .

4. Fluorescence studies in solution

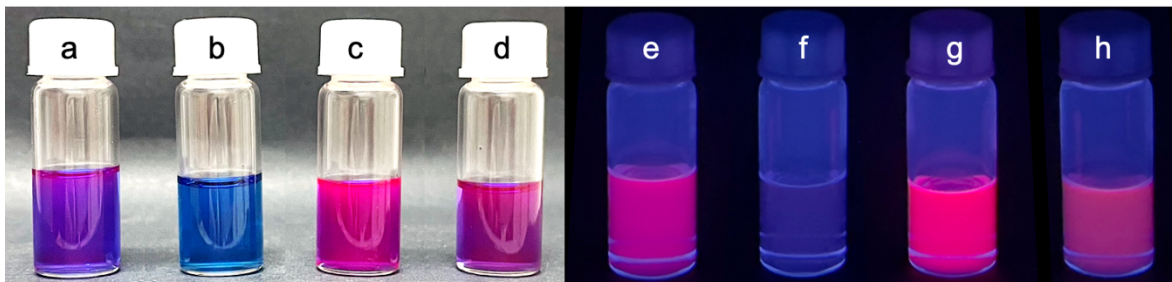


Fig. S7. Photographs of 8×10^{-5} M solutions of NDI-1 in (a) chloroform and (b) MCH; and 5×10^{-5} M solutions of NDI-2 in (c) chloroform and (d) MCH. Fluorescence emission under UV lamp ($\lambda = 365$ nm) irradiation of 8×10^{-5} M solutions of NDI-1 in (e) chloroform and (f) MCH; and 5×10^{-5} M solutions of NDI-2 in (g) chloroform and (h) MCH.

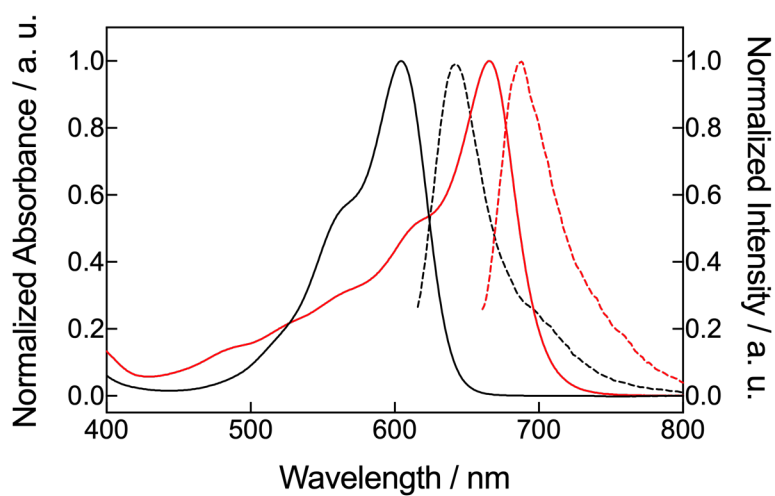


Fig. S8. Normalized emission (dotted lines) and absorption (solid lines) spectra of NDI-1 solutions in chloroform (black, $c = 5 \times 10^{-6}$ M) and MCH (red, $c = 5 \times 10^{-6}$ M).

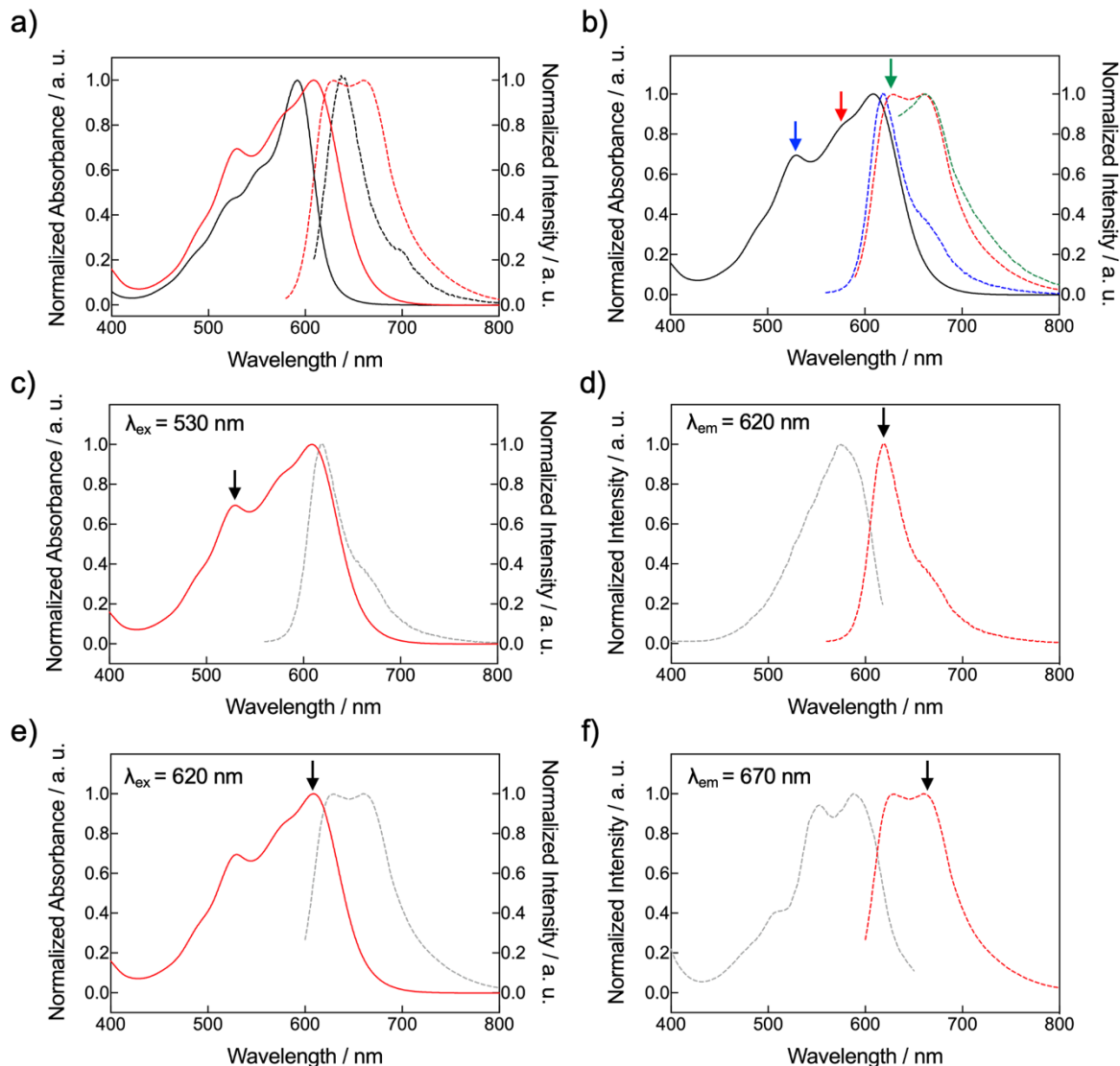


Fig. S9. (a) Normalized emission (dotted lines) and absorption (solid lines) spectra of NDI-2 solutions in chloroform (black, $c = 5 \times 10^{-6}$ M) and MCH (red, $c = 5 \times 10^{-6}$ M). (b) Normalized absorbance (black solid line) and emission spectra of NDI-2 solutions in MCH ($c = 5 \times 10^{-6}$ M) exciting at 530 nm (blue), 580 nm (red) and 630 nm (green). Vertical arrows indicate the excitation wavelengths corresponding with the color of the emission spectrum. (c) Normalized absorbance (solid red line) and emission (dotted grey line) spectra of NDI-2 solutions in MCH ($c = 5 \times 10^{-6}$ M). Inset indicates the excitation wavelength used to obtain the emission spectrum (marked with the black arrow). (d) Normalized emission (dotted red line) and excitation (dotted grey line) spectra of NDI-2 solution in MCH ($c = 5 \times 10^{-6}$ M). Inset indicates the emission wavelength used in the excitation spectrum (marked with the black arrow). (e) Normalized absorbance (solid red line) and emission (dotted grey line) spectra of NDI-2 solutions in MCH ($c = 5 \times 10^{-6}$ M). Inset indicates the excitation wavelength used in the emission spectrum (marked with the black arrow). (f) Normalized emission (dotted red line) and excitation (dotted grey line) spectra of NDI-2 solutions in MCH ($c = 5 \times 10^{-6}$ M). Inset indicates the emission wavelength used in the excitation spectrum (marked with the black arrow).

The NDI-2 sample was prepared by heating the MCH solution to 90 °C followed by cooling to room temperature. Based on the absorption and emission spectra

presented in Figure S9, this sample presents the coexistence of two (or more) aggregated species. The following observations on the fluorescence experiments were made:

- **Emission spectra:** When the sample was excited at 530 nm, it emitted a band with a maximum at 620 nm and a smaller peak (shoulder) at 670 nm (Figs S9b,c). This emission pattern was attributed to the emission of two aggregates: a first aggregate (AggA) with an absorption peak of around 530 nm and an emission band at 620 nm; and a J-aggregate with an absorption maximum at 610 nm and two emission peaks around 630 nm and 670 nm. Conversely, when the sample was excited at 580 or 620 nm, two emission bands of similar intensity were observed at 630 and 670 nm (Figs 9a,b,e). This emission pattern was attributed to the contribution of both aggregates, while each contribution could not be unveiled since depends on the quantum yield of each aggregate, which was not possible to measure. Furthermore, when the sample was excited at 630 nm, only the emission band at 670 nm was observed, while the band at 630 nm was below the measurable spectral range (Fig. S9b).
- **Excitation spectra:** The excitation spectra obtained at an emission wavelength of 620 nm exhibited a broad band ranging from 450 to 600 nm, peaking at 580 nm (Fig. S9d). This pattern was consistent with the absorption profile of the J-aggregate. In contrast, the excitation spectra at an emission wavelength of 670 nm displayed a three-peak pattern with maxima at 510 nm, 550 nm, and 620 nm (Fig. S9f). This profile was attributed to the sum of the absorption profiles of the J-aggregate and the AggA. From this experiment, we can deduce that the AggA may present two absorption maxima at 510 and 550 nm, which are not present in the J-aggregated species. However, it is apparent that this sample is complex, and therefore we cannot discard that other emissive NDI-2 species are present in the system.

Confocal microscope images (Fig. S10) supported the presence of at least two aggregates in the NDI-2 samples in MCH.

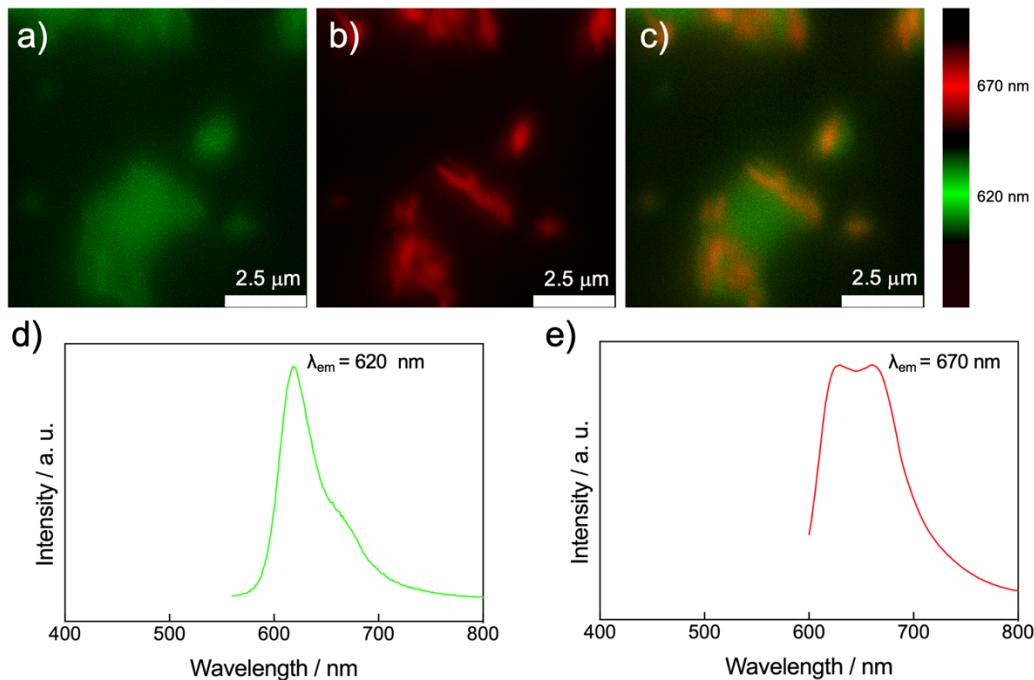


Fig. S10. Confocal microscope images ($\lambda_{ex} = 532 \text{ nm}$) of a drop-casted $5 \mu\text{M}$ solution of NDI-2 in MCH deposited between two glass plates. The images were recorded, after the sample was dried at open air, at **(a)** the range of 610 nm to 630 nm, **(b)** the range of 660 nm to 680 nm, and **(c)** superposition of the images (a) and (b). The scale bar (right) indicates the relationship between the color and the wavelength emission regions under excitation at 532 nm. **(d)** Emission spectra of the green areas (see image **(a)**) with the emission maxima at 620 nm. **(e)** Emission spectra of the red areas (see image **(b)**) with the emission maxima at 670 nm.

5. UV/vis studies in solution

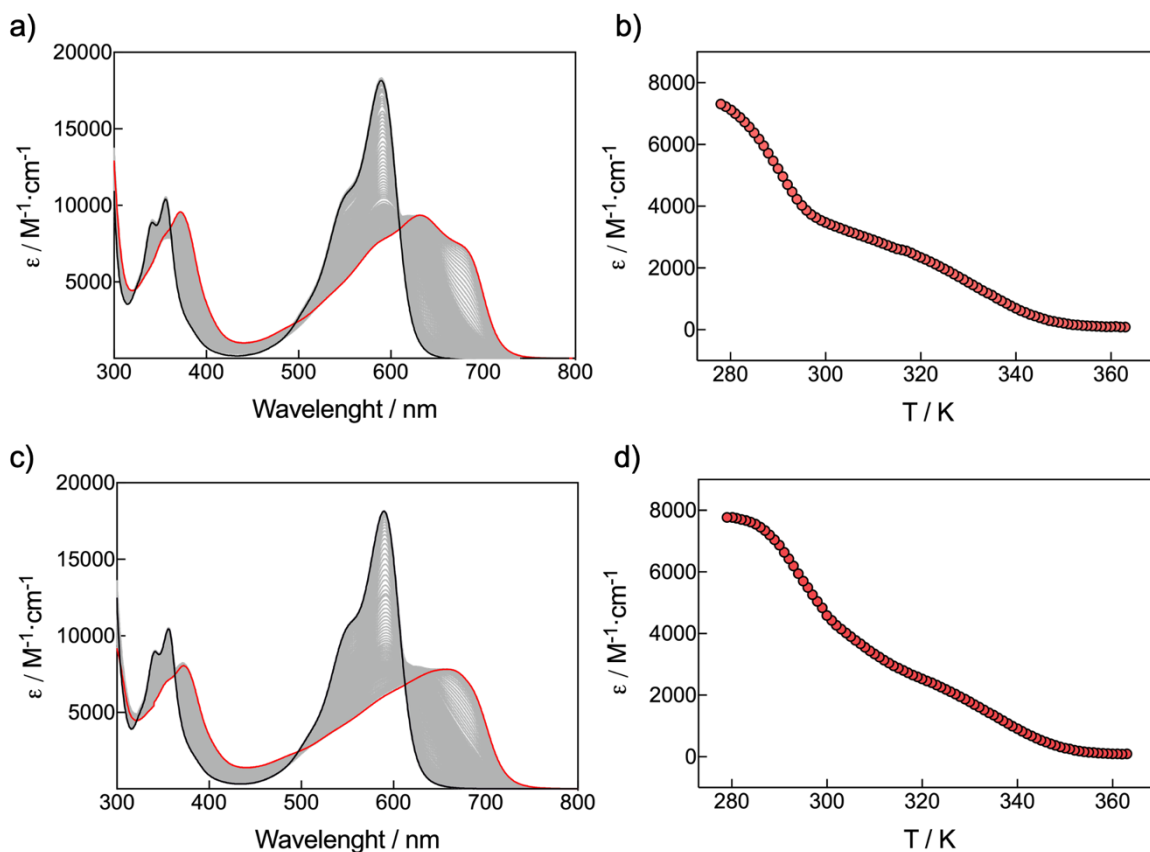


Fig. S11. (a) Temperature-dependent UV/vis experiment of the NDI-1 solution ($c = 8 \times 10^{-5}$ M) in MCH from 90 °C (black line) to 5 °C (red line) using a cooling rate of 1 $\text{K}\cdot\text{min}^{-1}$. (b) Molar extinction coefficient (ϵ) at 665 nm against the temperature of the NDI-1 ($c = 8 \times 10^{-5}$ M) solution in MCH from 90 °C to 5 °C using a cooling rate of 1 $\text{K}\cdot\text{min}^{-1}$. (c) Temperature-dependent UV/vis experiment of the NDI-1 solution ($c = 8 \times 10^{-5}$ M) in MCH from 90 °C (black line) to 5 °C (red line) using a cooling rate of 0.1 $\text{K}\cdot\text{min}^{-1}$. (d) Molar extinction coefficient (ϵ) at 665 nm against the temperature of an NDI-1 ($c = 8 \times 10^{-5}$ M) solution in MCH from 90 °C to 5 °C using a cooling rate of 0.1 $\text{K}\cdot\text{min}^{-1}$.

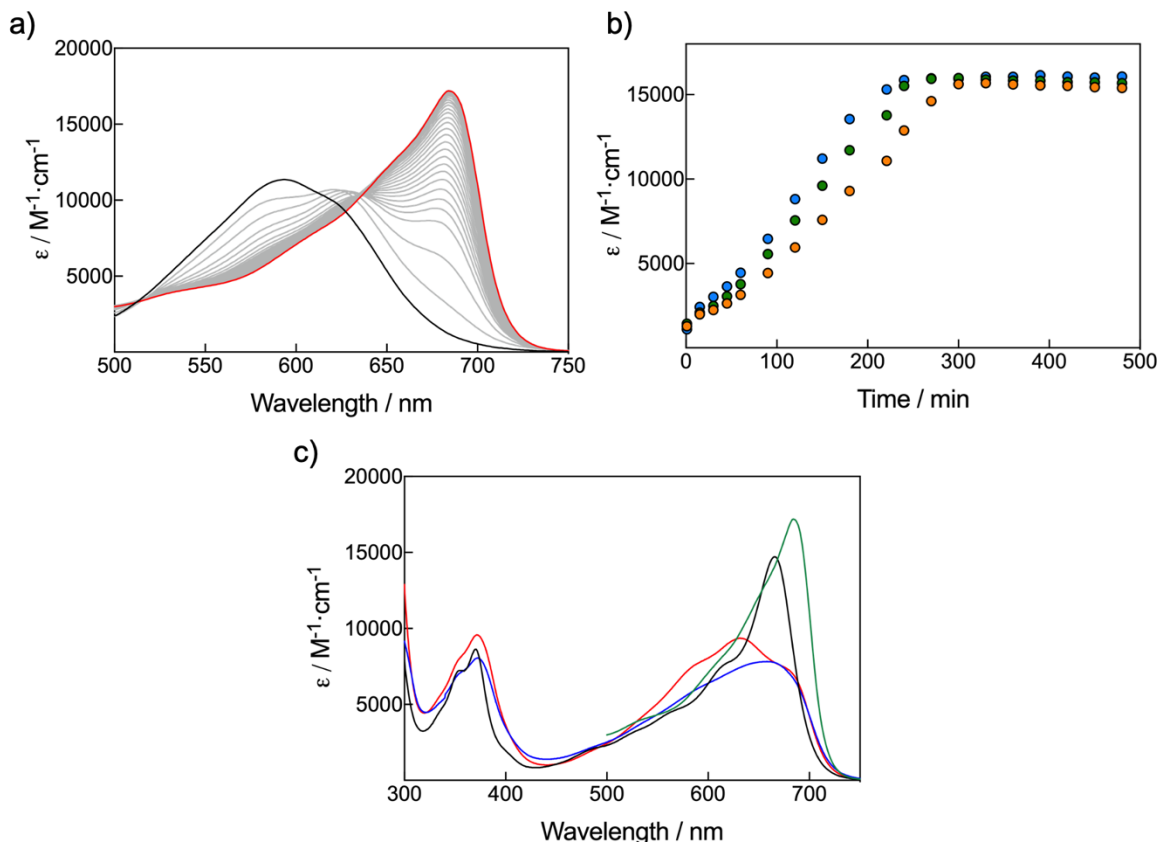


Fig. S12. (a) Time-dependent UV/vis experiment of an NDI-1 solution (8×10^{-5} M) in MCH at rt after fast cooling of the sample from 90 °C (temperature shock experiment) to 25 °C. Black line corresponds to the $t = 0$ min and red line to $t = 500$ min after the sample reached the 25 °C after the fast cooling process. (b) Molar extinction coefficient (ϵ) at 680 nm against the time of a 2×10^{-5} M (orange dots), 4×10^{-5} M (green dots) and 8×10^{-5} M (blue dots) NDI-1 solutions in MCH. (c) Comparison UV/vis spectra of NDI-1 in MCH: after directly dissolving the solid (black line); after heating to 90 °C and cooling at 1 K/min (red line) and at 0.1 K/min (blue line); and after fast cooling the sample (90 °C \rightarrow 25 °C) and waiting 500 min until the equilibria was reached (green line).

NDI-1 samples subjected to temperature-dependent experiments (Figs S11 and S12c) did not reach the equilibria state due to the formation of a kinetically trapped J-aggregate ($\lambda_{\text{max}} = 630$ nm). On the other hand, the thermal shock experiment demonstrates the formation of the thermodynamic J-aggregate ($\lambda_{\text{max}} = 690$ nm) after waiting 500 minutes at 25 °C. Through this process was reached the stronger J-coupling for the NDI-1, with the band J-band appearing at 690 nm. Lastly, the sample directly dissolved in MCH exhibits the absorption profile of a J-aggregate with a maximum at 670 nm. This latter sample is under thermodynamic conditions and remains unchanged over time (4 weeks), but it displays the absorption maxima at lower wavelengths compared to the J-aggregate obtained in the kinetic experiments. This discrepancy in the absorption profile was attributed to structural defects or the presence of trapped species in this sample directly prepared from the solid material.

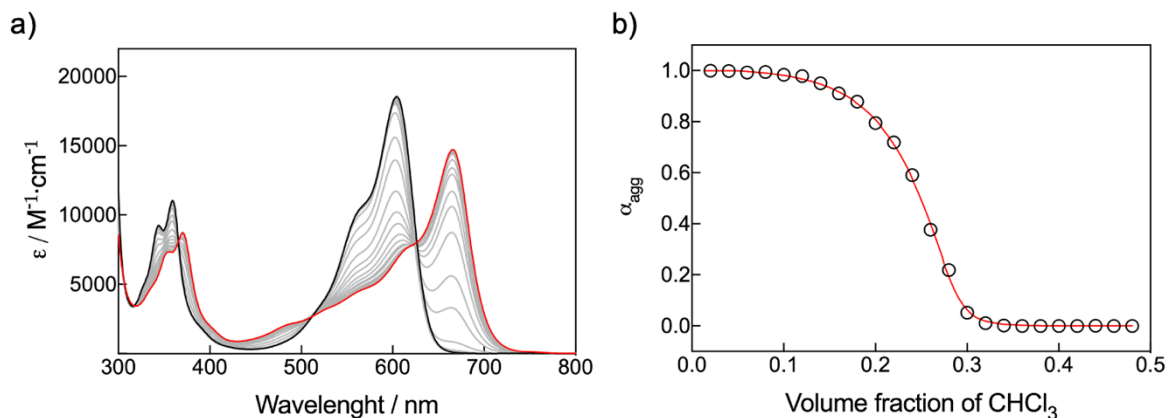


Fig. S13. (a) Denaturation UV/vis experiment of 8×10^{-5} M solutions of NDI-1 in chloroform/MCH. The solvent mixture ratio of CHCl_3 :MCH used was from a 0:100 (red line) to 50:50 (black line). **(b)** Degree of aggregation (α_{agg}) against the volume fraction of CHCl_3 in a CHCl_3 /MCH mixture (black dots) and the corresponding fitting curve (red line) obtained from the denaturation model for NDI-1 (see table S1). The degree of aggregation was calculated from the ϵ at 665 nm.

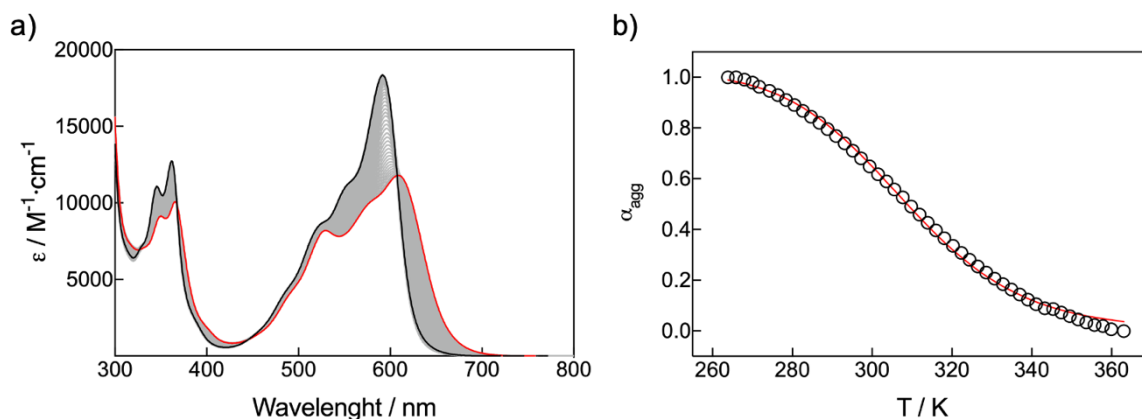


Fig. S14. (a) Temperature-dependent UV/vis experiment of a 1×10^{-4} M NDI-2 solution in MCH from 90 °C (black line) to -5 °C (red line) using a cooling rate of $0.1 \text{ K} \cdot \text{min}^{-1}$. **(b)** Degree of aggregation (α_{agg}) against temperature for NDI-2 in MCH (black dots) and the corresponding fit curve (red line) to the isodesmic model (see table S2). For the fitting we used the nucleation-elongation equation (see below) obtaining a $\sigma = 1$. The degree of aggregation was calculated from the ϵ at 620 nm.

Denaturation model for cooperative supramolecular polymerizations

Denaturation model is based on the study of the supramolecular polymerization as function of the chloroform volume fraction described by Meijer.^{S4} The data was analyzed expanding the nucleation-elongation model described by Goldstein and Stryer.^{S5}

$$[P_n] = K_n[P_{n-1}][X]$$

$$[P_{n+1}] = K_e[P_n][X]$$

$$[P_i] = K_e[P_{i-1}][X]$$

For the cooperative model $K_n < K_e$ and for isodesmic process $K_n = K_e$. The concentration for each species P_i is given by $[P_i] = K_n^{i-1}[X]^i$ for $i \leq n$ and $[P_i] = K_e^{i-n}K_n^{n-1}[P_{n-1}][X]$ for $i > n$.

The dimensionless mass balance is obtained by inserting the dimensionless concentration $p_i = K_e[P_i]$, the monomer concentration $x = K_e[X]$ and the concentration of each species $P_i (i \leq n): p_i = \sigma^{i-1}x^i$ and $P_i (i > n): p_i = \sigma^{n-1}x^i$:

$$x_{tot} = \sigma^{-1} \sum_{i=1}^n i(\sigma x)^i + \sigma^{n-1} \sum_{i=n+1}^{\infty} ix^i$$

Both sums are evaluated by standard expressions for converging series:

$$x_{tot} = \left(\frac{(\sigma x)^{n+1}(n\sigma - n - 1)}{(\sigma x - 1)^2} + \frac{\sigma x}{(\sigma x - 1)^2} \right) - \sigma^{n-1} \left(\frac{x^{n+1}(nx - n - 1)}{(x - 1)^2} \right)$$

Where $x_{tot} = c_{tot}K_e$ and c_{tot} : total monomer concentration.

The sum solved by standard numerical methods (Matlabfzerosolver) yields the dimensionless monomer concentration x . Considering that every species with $i > 1$ is defined as aggregate, the degree of aggregation results in:

$$\alpha_{agg} = \frac{x_{tot} - x}{x_{tot}}$$

Via $K_e = e^{-\frac{\Delta G^\circ}{RT}}$, the denaturation curves can be obtained with f , defined as volume fraction of good solvent:

$$\Delta G^{o'} = \Delta G^\circ + mf$$

It is assumed that the cooperativity factor σ is independent on the volume fraction and the m value for the elongation regime equals the m value for nucleation. The denaturation data need to be transformed into the normalized degree of aggregation, if fitted to the supramolecular polymerization equilibrium model:

$$(f) = \frac{A(f) - A(f = 0)}{A(f = 1) - A(f = 0)}$$

The optimization of the four needed parameters (ΔG° , m , σ and p) to fit the equilibrium model to the experimental data (normalized degree vs f) is done by the non-linear least-squares analysis using Matlab (lsqnonlinsolver). The data is then fitted with the non-linear least squared regression (Lavenberg-Marquard algorithm).

Table S1. Thermodynamic parameters (Gibbs free energy (ΔG°), m -factor (m) and cooperativity factor (σ)) obtained in denaturation fitting curves for NDI-1 (followed at 665 nm).

Parameter	NDI-1 ($c_{tot} = 8 \times 10^{-5}$ M)
T / K	298
n	2
$\Delta G^\circ / \text{kJ} \cdot \text{mol}^{-1}$	-37.3 ± 0.6
$m / \text{kJ} \cdot \text{mol}^{-1}$	50 ± 2
σ	0.018 ± 0.008 (cooperative)

Nucleation-elongation model for supramolecular polymerizations

The equilibrium between the monomeric and supramolecular polymer species can be described with the Nucleation-Elongation model, which was developed by Ten Eikelder, Markvoort and Meijer.^{S6} This model is used to describe the aggregation of NDI-2. The model extends nucleation-elongation based equilibrium models for growth of supramolecular homopolymers to the case of two monomer and aggregate types and can be applied to symmetric supramolecular copolymerizations, as well as to the more general case of nonsymmetric supramolecular copolymerizations.

In a cooperative process, the polymerization occurs via two steps: a nucleation step, where a nucleus, which is assumed to have a size of two molecules, is formed and a following elongation step. In anisodesmic process, the polymerization occurs via elongation step. The values T_e , ΔH_n° , ΔH° and ΔS° can be found by a non-linear least-squares analysis of the experimental cooling curves. The equilibrium constants associated with the nucleation and elongation phases can be calculated using the following equations:

Nucleation step:

$$K_n = e^{-\frac{(\Delta H^\circ - \Delta H_n^\circ) - T\Delta S^\circ}{RT}}$$

Elongation step:

$$K_e = e^{-\frac{\Delta H^\circ - T\Delta S^\circ}{RT}}$$

Furthermore, the cooperativity factor is given. By:

$$\sigma = \frac{K_n}{K_e}$$

Where $K_n < K_e$ ($\sigma < 1$) in a cooperative process and for isodesmic process $K_n = K_e$ ($\sigma = 1$).

Table S2. Thermodynamic parameters (standard enthalpy (ΔH°), standard entropy (ΔS°), nucleation enthalpy (ΔH_n°), elongation temperature (T_e), elongation (K_e) and nucleation (K_n) binding constants, and cooperativity factor (σ) inferred for NDI-2 in MCH as solvent.

Parameter	NDI-2 ($\lambda = 620$ nm)
$\Delta H^\circ / \text{kJ}\cdot\text{mol}^{-1}$	-58.2 ± 1
$\Delta S^\circ / \text{J}\cdot\text{mol}^{-1}\cdot\text{K}^{-1}$	-0.113 ± 0.004
$\Delta H_n^\circ / \text{kJ}\cdot\text{mol}^{-1}$	0.00 ± 0.08
T_e / K	301.0 ± 0.5
N	16469.6
$\Delta G^\circ / \text{kJ}\cdot\text{mol}^{-1}$	-24.58
K_e	16129.92
K_n	16129.92
σ	1 (isodesmic)

6. Morphology studies of the supramolecular polymers

Sample preparation

50 μL of a previously prepared 8×10^{-5} M of **NDI** in MCH were spin-coated onto mica surface. Then, the mica was dried with an argon flux for 5 min.

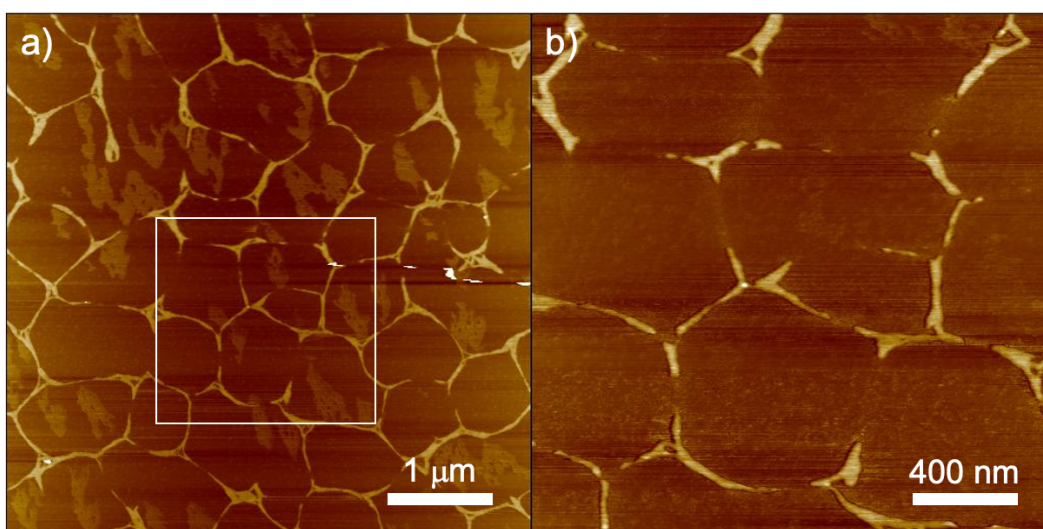


Fig. S15. (a) Atomic force microscopy image of a spin-coated solution of NDI-1 in MCH ($c = 8 \times 10^{-5}$ M) on mica surface. (b) Magnification of the white square indicated in image (a).

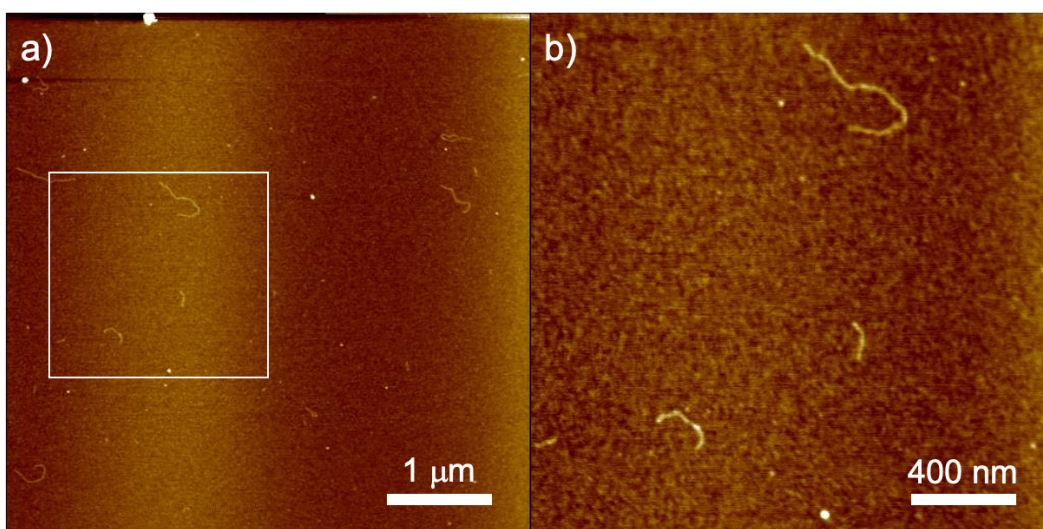


Fig. S16. (a) Atomic force microscopy image of a spin-coated solution of NDI-2 in MCH ($c = 5 \times 10^{-5}$ M) on mica surface. This sample was prepared by dissolving the solid NDI-2 in MCH and then heating the sample to $90\text{ }^\circ\text{C}$ and then cooling to r.t. (b) Magnification of the white square indicated in image (a).

7. DSC experiments

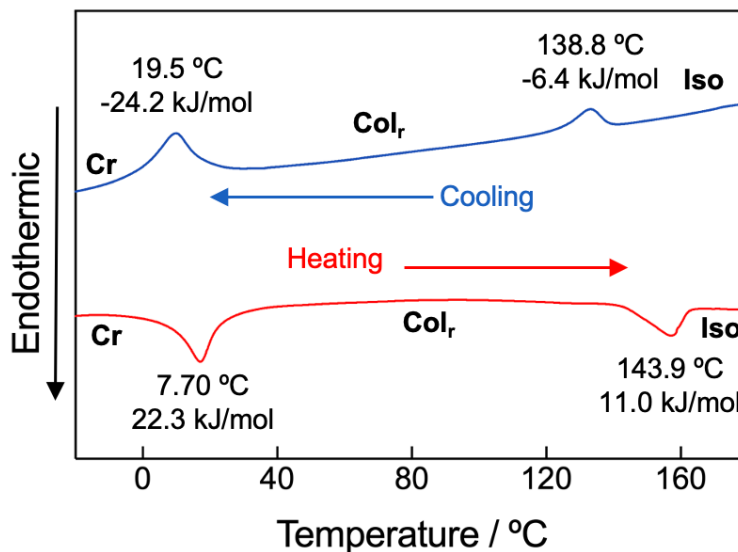


Fig. S17. Differential scanning calorimetry traces on a first cooling (blue line) and second heating (red line) of NDI-1. Heating/cooling rate 10 °C min⁻¹. Transition temperatures indicated correspond to the onset values.

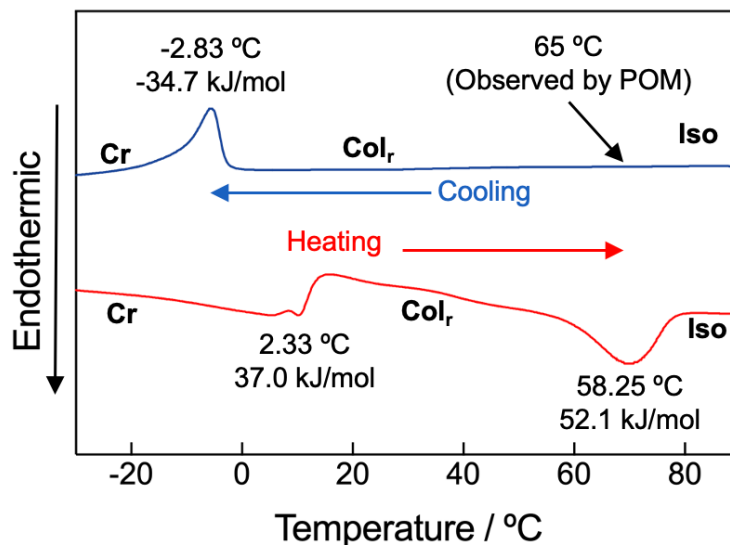


Fig. S18. Differential scanning calorimetry traces on a first cooling (blue line) and second heating (red line) of NDI-2. Heating/cooling rate 10 °C min⁻¹. Transition temperatures indicated correspond to the onset values.

8. X-ray studies

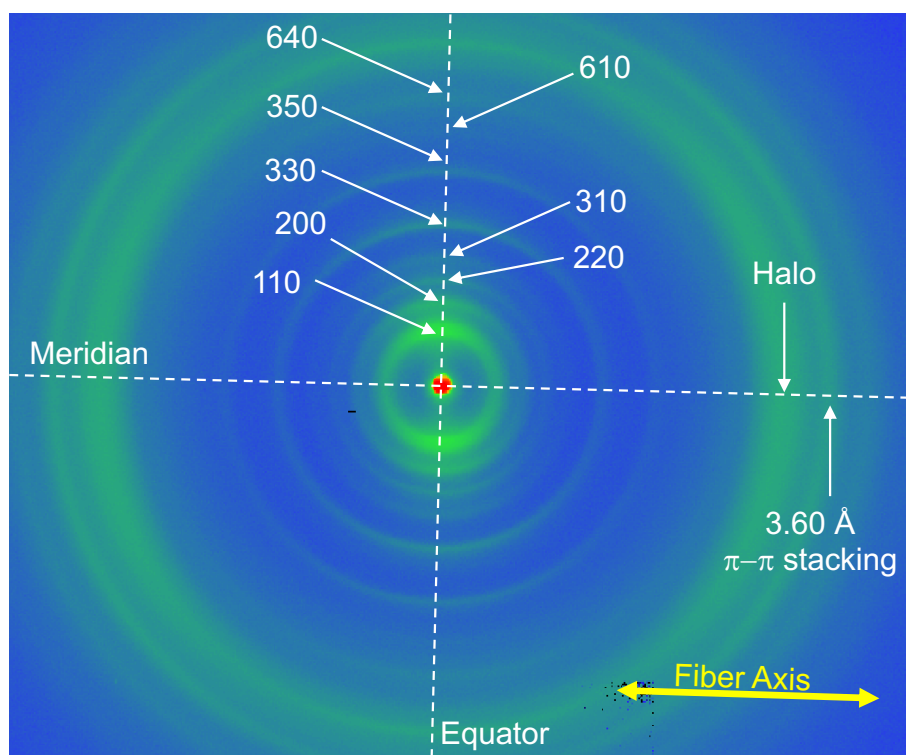


Fig. S19. MAXS pattern of an extruded sample of NDI-2 at 65 °C. The fiber was only partly aligned.

Data analysis

The X-ray data was analyzed using the Datasqueeze 3.0 Software.^{S7} The calculated interplanar spacing distances for a columnar rectangular mesophases (d_{hko}) were obtained according to the following equation:^{S8}

$$\frac{1}{d_{hko}^2} = \frac{h^2}{a^2} + \frac{k^2}{b^2}$$

Where a and b are de lattice parameters obtained from the MAXS experiments; h and k are de Miller indices.

Table S3. Experimental and calculated interplanar spacing distances for the Col_r phases of NDI-1 and NDI-2.

Compound	Phase	Lattice parameters	Reflection	hkl	$d_{exp} / \text{Å}$	$d_{calc} / \text{Å}$
NDI-1	Col _r (<i>c2mm</i>)	$a = 59.7 \text{ Å}$ $b = 42.7 \text{ Å}$	1	110	35.02	34.73
			2	200	29.65	29.85
			3	020	21.22	21.35
			4	130	13.92	13.85
			5	510	11.41	11.50
			6	150	8.38	8.38
NDI-2	Col _r (<i>p2mm</i>)	$a = 34.7 \text{ Å}$ $b = 40.7 \text{ Å}$	1	110	26.41	26.35
			2	200	17.35	17.18
			3	220	13.20	13.31
			4	310	11.13	11.09
			5	330	8.80	8.83
			6	350	6.66	6.69
			7	600	5.78	5.58
			8	640	5.03	5.08

Calculation of the number of molecules per columnar stratum

The number of molecules (Z) per columnar stratum was calculated as reported previously, using equation:^{S9}

$$Z = \frac{\rho \cdot N_A \cdot V_{col-strat}}{M_w}$$

where ρ indicates the density (assuming $0.8\text{-}1 \text{ g}\cdot\text{cm}^{-3}$), N_A is the Avogadro's constant ($6.022 \cdot 10^{23} \text{ molecules}\cdot\text{mol}^{-1}$), M_w is the molecular mass of NDI and $V_{col-strat}$ is the volume of the columnar stratum. To calculate the $V_{col-strat}$ was used the equation:^{S10}

$$V_{col-strat} = \frac{a \cdot b \cdot h}{n}$$

where a and b are de lattice parameters obtained from the MAXS experiments, h is the size of the repeating unit and n is the discoid number of the column ($n = 1$ in the case of *p2mm* symmetry group and $n = 2$ in the case of *c2mm* symmetry group).^{S8}

Table S4. Number of molecules (Z) per columnar stratum values for NDI-1 and NDI-2.

Compound	$\rho / \text{g}\cdot\text{cm}^{-3}$	a / cm	b / cm	h / cm	n	$V_{col-strat} / \text{cm}^3$	Z
NDI-1	0.85	59.7×10^{-8}	42.7×10^{-8}	10×10^{-8}	2	13816	4.1
NDI-2	0.85	42.2×10^{-8}	34.3×10^{-8}	3.4×10^{-8}	1	2711	1.4

9. Polarized experiments for NDI-1

Polarized UV/vis experiments

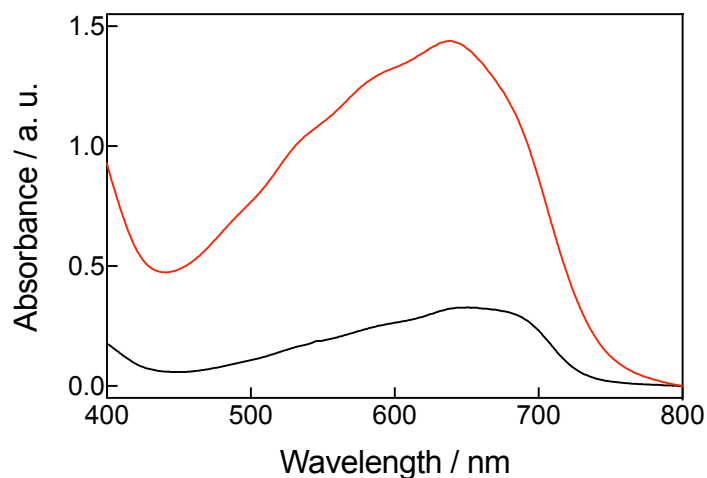


Fig. S20. Polarized UV/vis spectra of an aligned sample (mechanical shearing) of NDI-1 on a quartz plate acquired perpendicular (black) and parallel (red) to the aligning direction.

Polarizing Optical microscope studies

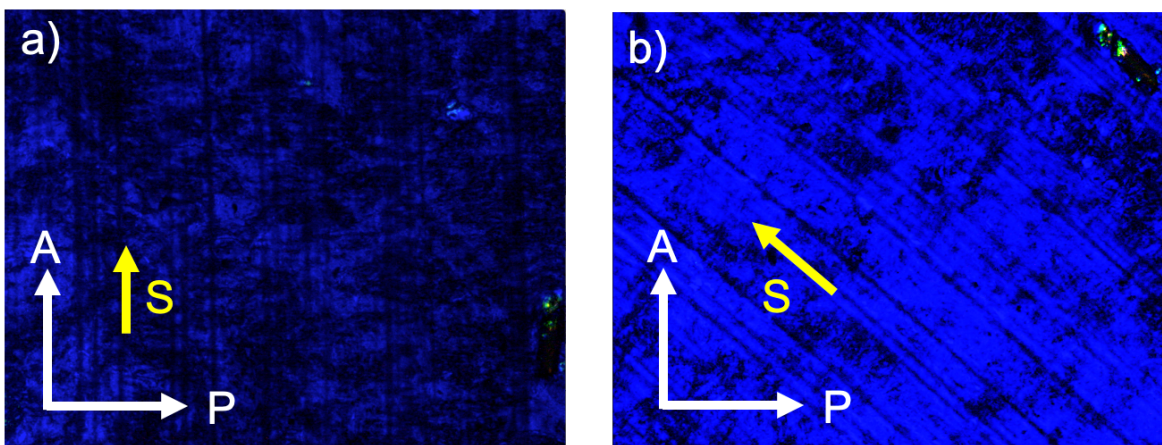


Fig. S21. Polarized optical microscopic images of NDI-1 after mechanical shearing with the Analyzer (a) parallel to the shearing direction and (b) after sample holder rotation of 45°.

10. Transition dipole moment for NDI-1

The transition dipole moment of NDI-1 was computed using ORCA 4.2 program^{S11} at the B3LYP^{S12}/def2-TZVP^{S13} level of theory using fully optimized models where the long dodecyloxy chains have been replaced by H-atoms. The plots shown in Fig. S22 have been generated using Avogadro 1.2.0 program.^{S14}

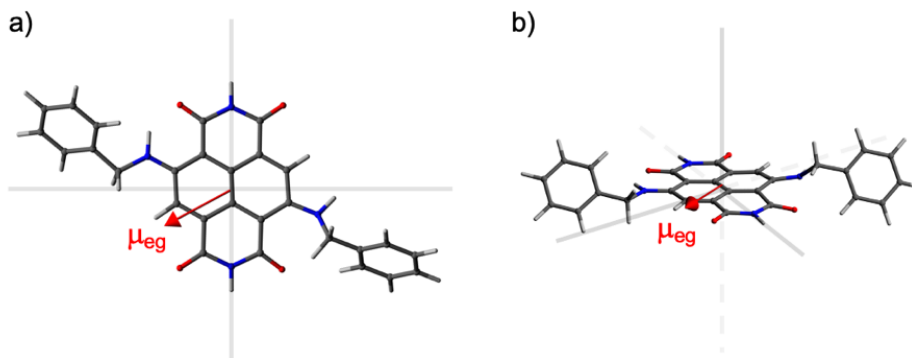


Fig. S22. Transition dipole moment (red arrow) direction of NDI-1 respect of the NDI core in a (a) top view and (b) side view. Grey lines correspond to a cartesian axes respect the NDI core plane.

Cartesian coordinates for the **NDI-1** model for transition dipole moment

C	-2.31950295883906	-3.22229838671058	1.08950754698033
C	-1.85864017047220	-1.84220237962338	0.77375964289401
C	-2.78924060894199	-0.85513882164332	0.32540498493326
C	-4.17494464959570	-1.16456080401642	0.11102237957261
C	-4.66272322246080	-2.48913456389572	0.55594807088805
C	-0.52255296704300	-1.55762672105976	0.96129871801597
C	-2.27401030536882	0.45603669511212	0.11967115782956
C	-0.89588617032921	0.76044808742375	0.31997145165511
C	0.01503428348892	-0.25551955335447	0.73145904344524
C	-0.42623446072827	2.13459157733908	0.10194045858202
C	-2.74607784193258	2.86820479050457	-0.49206269153290
C	-3.19885962649010	1.46597130631427	-0.28083430858880
C	-4.51922437551649	1.15965600062434	-0.51659427533277
C	-5.05013998795410	-0.15852523286106	-0.38399812637092
H	-5.17100736430249	1.96962493987599	-0.85552403684556
H	0.11143494200986	-2.37210954618525	1.31074039232068
N	-1.38853793546958	3.06652877813056	-0.27871993888611
N	-3.68645470643379	-3.40117283229240	0.96716092246814
O	-3.47460163862776	3.78217677821397	-0.82716020259313
O	0.73855005767076	2.50819296450970	0.23581204582582
O	-1.58925082098396	-4.12458138168679	1.45267362239715
O	-5.83362359752386	-2.83470517829753	0.61524190545353
H	-1.04507592938920	4.01451624786680	-0.42203480393354
H	-4.04689694399313	-4.31013507350120	1.25160002416701
N	-6.37413889444293	-0.30849766021442	-0.73054449787162
H	-6.82508013541640	0.58581836569487	-0.89996908138600
N	1.33336679109334	-0.00331176678895	0.91089700015345
H	1.60295450385055	0.97730432005134	0.80051948823193
C	2.31773507771850	-0.97491634188920	1.34963793343858
H	2.22385056384752	-1.89290184035349	0.73922934255146
H	2.13543375705194	-1.28365213937557	2.39669635773962
C	-6.96486379091228	-1.36255704574477	-1.55872172795631
H	-6.67958637079573	-1.21873523725695	-2.61937430002742
H	-6.57529228003607	-2.33057014074004	-1.22731876681975
C	-8.47304730703777	-1.35644441676150	-1.42829188538268

C	-9.29622866382692	-1.01584956764456	-2.51015374704426
C	-9.06763037068731	-1.69068009747304	-0.19881933634426
C	-10.68968858309994	-1.01081899654672	-2.37376456943181
H	-8.84365812130651	-0.75413819132405	-3.47170493290312
C	-10.45660875395650	-1.68386020551977	-0.06119611795212
H	-8.42373875994894	-1.96105312532942	0.64175361674840
C	-11.27192706439232	-1.34338620920175	-1.14831733487994
H	-11.31898398738775	-0.74368280354841	-3.22713025713346
H	-10.90908660839880	-1.95086568817632	0.89794265446226
H	-12.36009542813823	-1.33879687224624	-1.03822172470442
C	3.73303152263865	-0.44605264003464	1.22255594154004
C	4.13748952944504	0.28531040707703	0.09384132398944
C	4.67904713077290	-0.72234958630982	2.22077525149914
C	5.45701523220544	0.72846837927700	-0.03100297772343
H	3.41265271701846	0.51727095087725	-0.69066238540917
C	6.00137415880861	-0.28663180302052	2.09358129741475
H	4.37688820476446	-1.28289659405888	3.11057765592938
C	6.39420777941352	0.44190688125376	0.96681178774446
H	5.75431549185316	1.30030504214197	-0.91420541684286
H	6.72462669020272	-0.51142717597395	2.88216315724780
H	7.42579765832657	0.78989771837252	0.8686572777712

11. Fourier transform infrared spectroscopy experiments

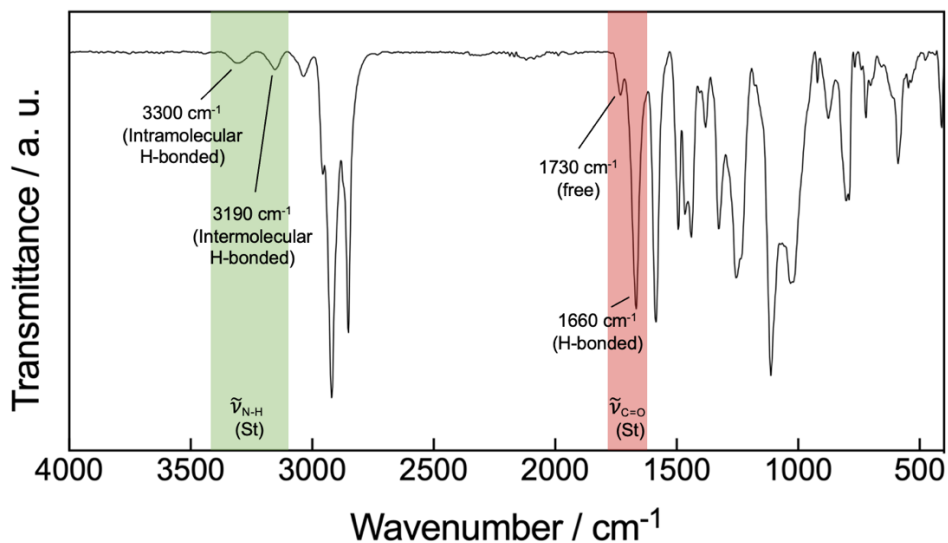


Fig. S23. Fourier transform infrared spectra of NDI-1 in solid state. Green region corresponds to the N-H stretching vibrations and red region indicates the C=O stretching (St) vibrations.

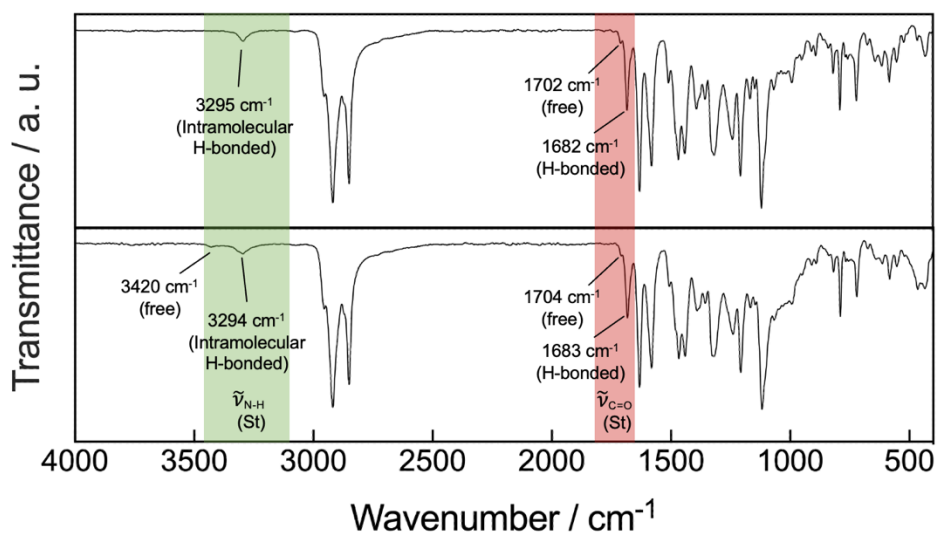


Fig. S24. Fourier transform infrared spectra of NDI-2 in solid state before (top) and after (down) mechanical shearing. Green region corresponds to the N-H stretching (St) vibrations and red region indicates the C=O stretching (St) vibrations.

12. Molecular modelling

Retrostructural analysis

The molecular structure of NDI-1 was geometry optimized with the Grimme's extended semiempirical tight-binding method (GFN2 xTB method)^{S15} and the optimized molecular structure was then imported to Avogadro 1.2.0.^{S14}

The fiber diffraction pattern of NDI-1 was simulated with CLEARER using the geometry optimized structure. The structure was exported as PDB-file and imported into the Fiber Diffraction Simulation module of CLEARER.^{S16} The fiber axis was set to (0,0,1) using the parameters of unit cell obtained in X-ray studies (see table S3). The contrast was adjusted to best visualize the signals of the pattern.

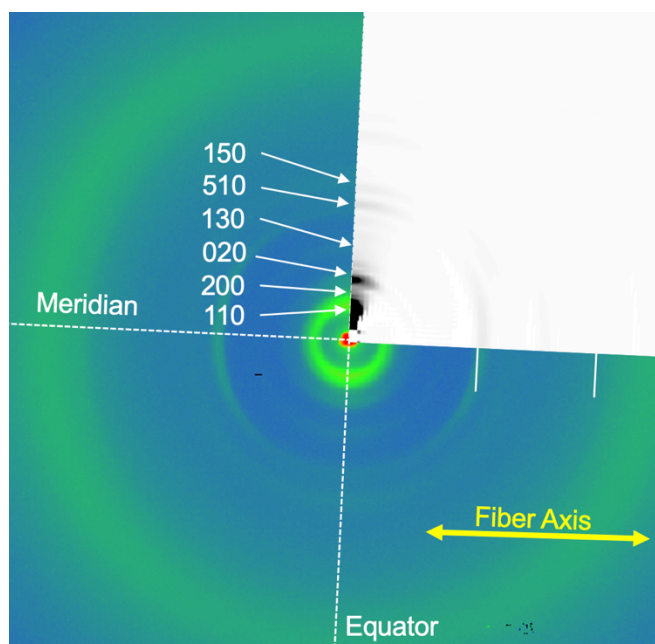


Fig. S25. MAXS pattern of an aligned fiber of NDI-1 and the superposed simulated pattern with CLEARER.^{S16}

Exciton coupling

For the exciton coupling calculations we utilized the data obtained from the UV/vis experiments.

Table S5. Optical properties of NDI-1 and NDI-2 in solution and solid state.

Compound	State	λ_{max} / nm	ϵ / L·mol ⁻¹ ·cm ⁻¹	FWHM* / cm ⁻¹	$\Delta\tilde{\nu}$ / cm ⁻¹
NDI-1	CHCl ₃ (sol.)	600	18200	1120	-
	MCH (sol.)	670	14400	1380	- 1541
	Solid	650	-	1240	-1172
NDI-2	CHCl ₃ (sol.)	590	17900	1080	-
	MCH (sol.)	610	12150	1530	-555
	Solid (unsheared)	580	-	1150	+292
	Solid (sheared)	640	-	1460	-1324

*Full width at half maximum (FWHM) was derived as twice the distance between the absorption maximum to the closest edge at half maximum of the unsymmetrically shaped absorption bands.

To explain the bathochromic shift of NDI UV/vis spectra of J-aggregate specie was calculated the exciton coupling energies using Kasha exciton theory^{S17}, according to the equation:

$$J_i = \frac{|\mu_{eg}|^2}{4\pi\epsilon_0 r_{c-c}^3} (\cos \alpha - 3\cos^2 \theta)$$

Where μ_{eg} is the transition dipole moment of the monomer, ϵ_0 is the permittivity in vacuum, r_{c-c} is the distance between neighboring molecule core centers, α is the angle formed by the transition dipole moments of two molecules arranged in parallel and θ is the angle resulting from the displacement of two parallel arranged molecules.

The angle θ and the distances r_{c-c} were obtained from the model of the Fig. 5e obtained with the Grimme's extended semiempirical tight-binding method (GFN2 xTB method)^{S15} from the center of one NDI to the center of the adjacent NDI molecule in π - π stack and hydrogen bond direction. The angle α has a value of 0. The transition dipole moment was obtained from the equation:

$$|\mu_{eg}|^2 = \frac{3hc\epsilon_0 \ln 10}{2\pi^2 N_A} \cdot \int_{\tilde{\nu}_1}^{\tilde{\nu}_2} \frac{\epsilon(\tilde{\nu})}{\tilde{\nu}} d\tilde{\nu}$$

Where $\epsilon(\tilde{\nu})$ is the molar extinction coefficient, c is the speed of the light, h is the Plank constant, N_A is the Avogadro number and $\int_{\tilde{\nu}_1}^{\tilde{\nu}_2} \frac{\epsilon(\tilde{\nu})}{\tilde{\nu}} d\tilde{\nu}$ is the integral of the reduced UV/vis absorption band of the monomer.

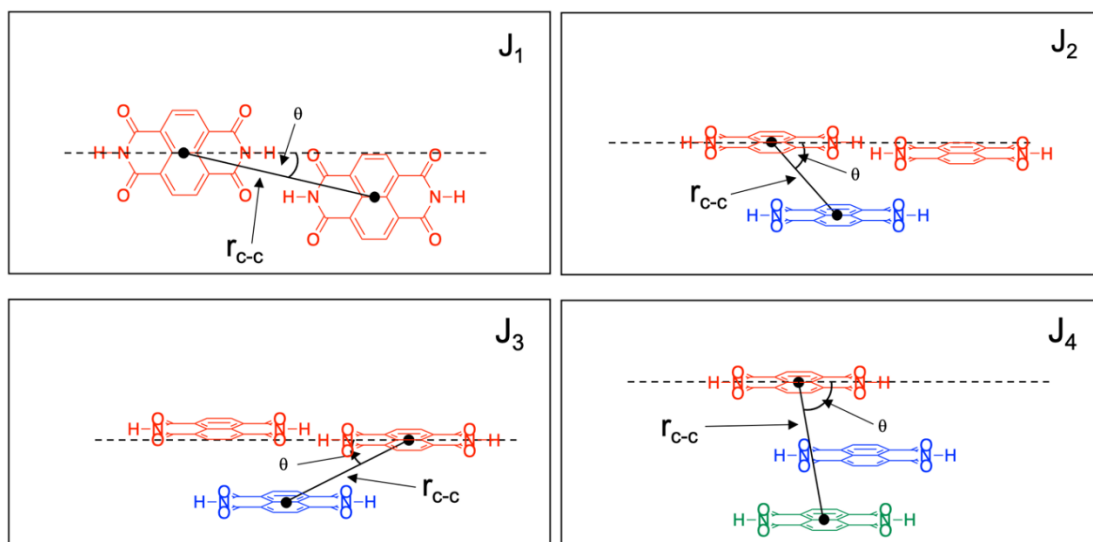


Fig. S26. Schematic representation of the exciton couplings present in a four stranded NDI-1 aggregate (extracted in a three strand section of the modeled structure Fig. 5e). Red structures represent the first strand, blue structures the second strand and green structures the third strand of the NDI-1 aggregate according with the supramolecular aggregation pattern.

Table S6. Transition dipole moment (μ_{eg}) and exciton coupling energies (J_i) of NDI-1 in hydrogen bond (J_1), slipped π - π stack (J_2 and J_3) and side-by-side stack (J_4) direction.

	μ_{eg} / D	$r_{c-c} / \text{\AA}$	$\theta / ^\circ$	J_i / cm^{-1}
J_1		10.04	16.2	- 174
J_2	4.4	6.87	26.8	- 426
J_3		5.00	38.3	- 674
J_4		7.05	70.9	+ 193

The sign (+/-) specifies the type of exciton coupling contribution, where a negative exciton coupling indicates a J-type coupling and a positive exciton coupling indicates a H-type coupling.

13. Mechanochromic experiments

Procedure for the mechanical shearing (rubbing)

A small amount of NDI-2 was deposited onto a square quartz plate and was rubbed with a spatula for 1 minute inducing the color change from blue to pink. The sample was heated to 60 °C for 1 minute and cooled at rt to reverse the process. The procedure was repeated few times to confirm its reversibility. Fluorescence was checked using a laboratory lamp ($\lambda = 356$ nm). For NDI-1, no fluorescence in solid-state was observed before and after shearing the sample.

Determination of fluorescence quantum yield

We could not determine the fluorescence quantum yields (Φ) of the solid NDI-2 before and after shearing, and instead, we calculated the quantum yields of these two samples after dissolving them in MCH. The dissolution in MCH of the NDI-2 LC H-aggregate (before shearing) provided a UV/vis profile consistent with an H-aggregate, while the solubilization of the sheared sample provided a profile showing a slightly coupled J-aggregate. The results are shown in the Figure S27.

The fluorescence quantum yields of these samples in MCH were calculated using the Resch-Genger method.^{S18} For the measurements Rhodamine 6G was used as standard. The results of the fluorescence quantum yield are indicated as inset of the Figs 27a (H-aggregate) and 27b (J-aggregate).

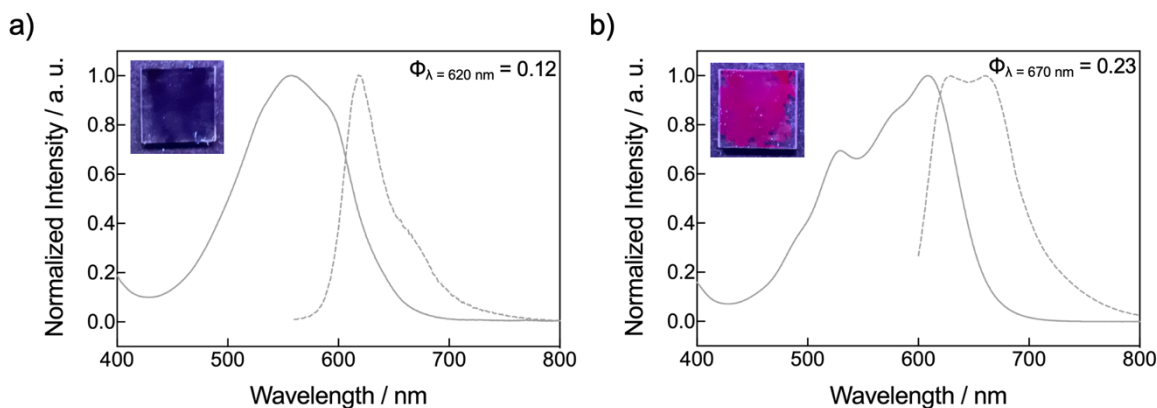


Fig. S27. (a) Normalized UV/vis (solid grey line, $c = 5 \times 10^{-5}$ M) and fluorescence emission spectra (dotted line, $c = 5 \times 10^{-6}$ M, $\lambda_{\text{ex}} = 550$ nm) of the directly solubilized LC NDI-2 in MCH. Inset shows a thin film of NDI-2 onto a quartz substrate before mechanical shearing. The quantum yield at 620 nm is indicated inset. (b) Normalized UV/vis (solid line, $c = 5 \times 10^{-5}$ M) and fluorescence emission spectra (dotted line, $c = 5 \times 10^{-6}$ M, $\lambda_{\text{ex}} = 600$ nm) of the sheared sample of NDI-2 solubilized in MCH. Inset shows a thin film of NDI-2 onto a quartz substrate after mechanical shearing. The quantum yield of NDI-2 at 670 nm is indicated inset.

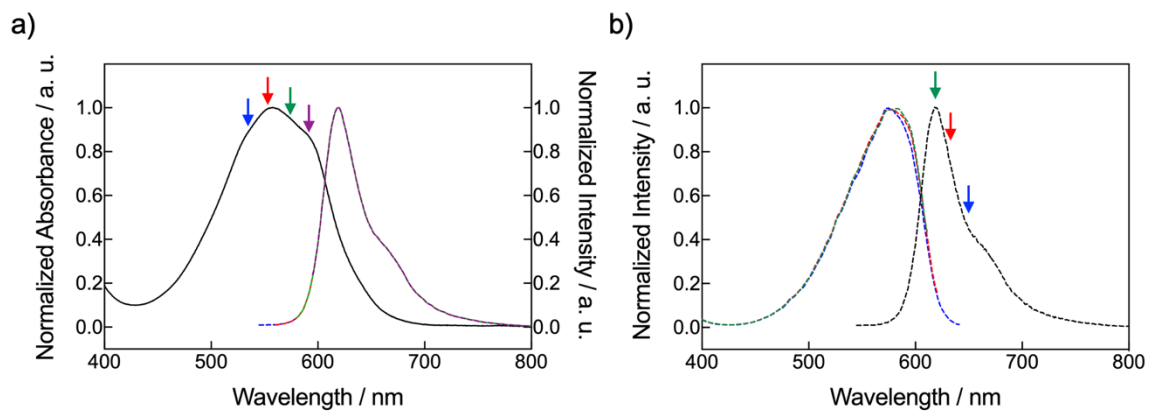


Fig. S28. (a) Normalized absorbance (black solid line) and emission spectra (dotted lines) of NDI-2 solutions in MCH ($c = 5 \times 10^{-6}$ M) exciting at 530 nm (blue), 550 nm (red), 570 nm (green) and 590 nm (purple). Vertical arrows indicate the excitation wavelengths corresponding with the color of the emission spectrum. **(b)** Normalized emission (black dotted line) and excitation spectra (dotted lines) of NDI-2 solutions in MCH ($c = 5 \times 10^{-6}$ M) emitting at 650 nm (blue), 630 nm (red), 620 nm (green). Vertical arrows indicate the emission wavelengths corresponding with the color of the emission spectrum.

X-ray studies

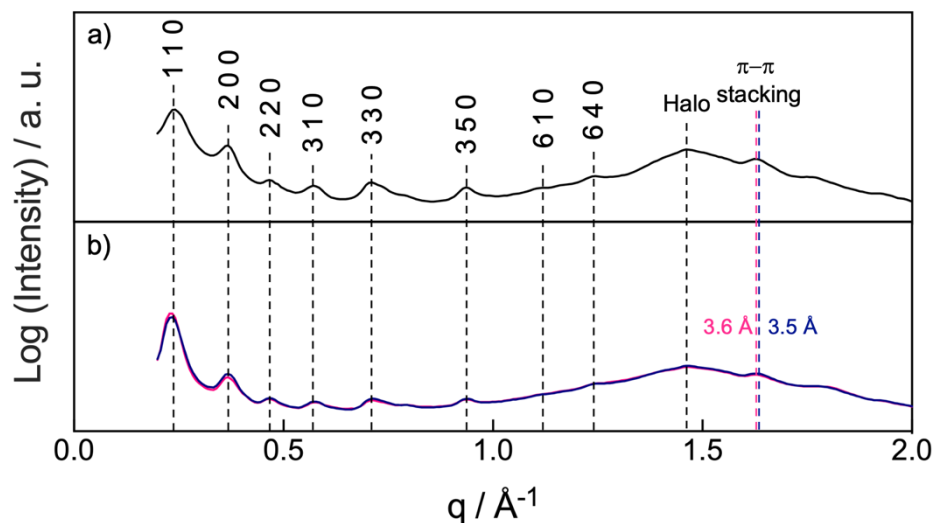


Fig. S29. X-ray patterns of NDI-2 at 25 °C of (a) an unsheared sample, (b) a mechanically sheared sample before (pink line) and after (blue line) a process of thermal annealing (25 °C → 60 °C (10 min) → 25 °C). These two later spectra were taken exactly on the same sample spot. All the measurements were conducted by depositing the sample into a borosilicate glass capillary.

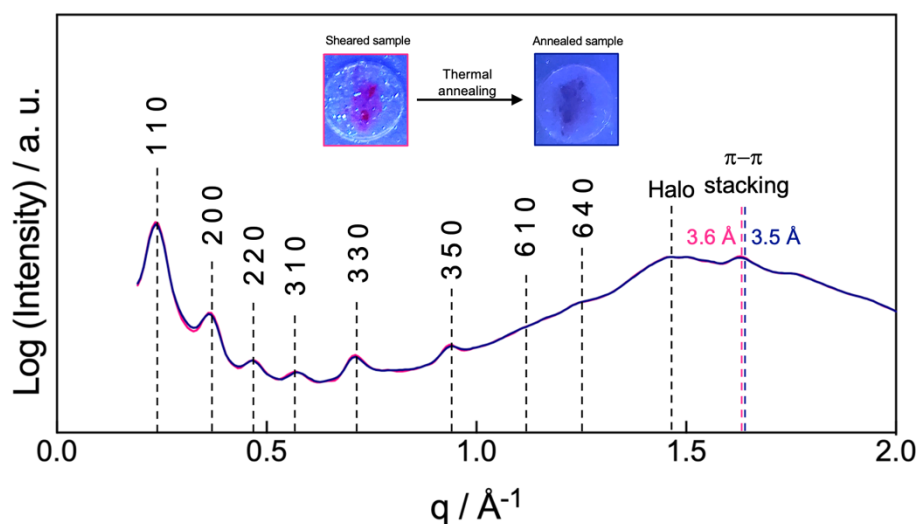


Fig. S30. X-ray patterns of a mechanically sheared sample of NDI-2 at 25 °C before (pink line) and after (blue line) the thermal annealing (25 °C → 60 °C (10 min) → 25 °C). Both spectra were taken exactly on the same sample spot. Insets show the samples sandwiched between two glass plates and irradiated by a 365 nm laboratory lamp irradiation. The shearing of the sample was performed by moving the two glasses sandwiching the sample, and the measurements were taken in the same glasses.

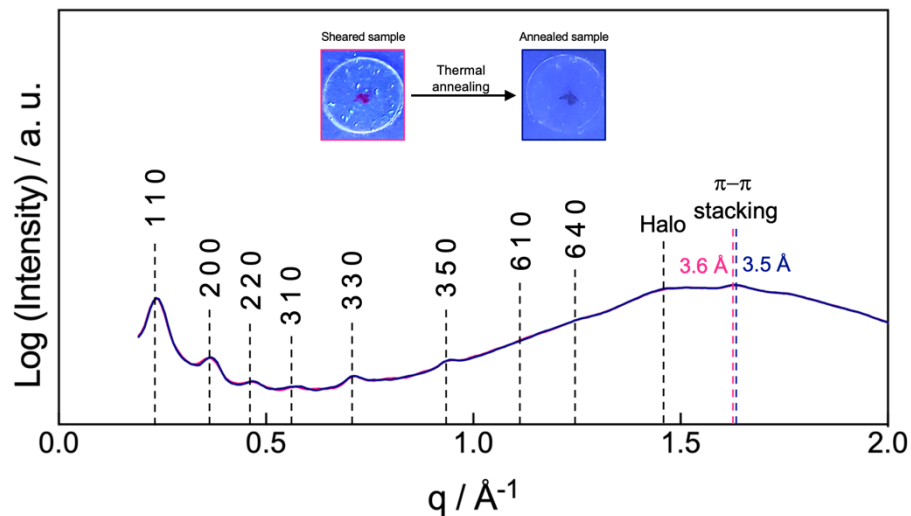


Fig. S31. X-ray patterns of a mechanically sheared sample of NDI-2 at 25 °C before (pink line) and after (blue line) the thermal annealing (25 °C → 60 °C (10 min) → 25 °C). Both spectra were taken exactly on the same sample spot. Insets show the samples sandwiched between two glass plates and irradiated by a 365 nm laboratory lamp irradiation. The sample was sheared using two microscope slides and then transferred onto the glass plates for the measurements.

14. References

- S1.** H. Kar, W. Gehrig, K. Allampally, G. Fernández, F. Laquai and S. Ghosh, *Chem. Sci.*, 2016, **7**, 1115-1120.
- S2.** X. Lu, W. Zhu, Y. Xie, X. Li, Y. Gao, F. Li and H. Tian, *Chem. Eur. J.*, 2010, **16**, 8355-8364.
- S3.** V. Percec, M. Peterca, T. Tadjiev, X. Zeng, G. Ungar, P. Leowanawat, E. Aqad, M. R. Imam, B. M. Rosen, U. Akbey, R. Graf, S. Sekharan, D. Sebastiani, H. W. Spiess, P. A. Heiney and S. D. Hudson, *J. Am. Chem. Soc.*, 2011, **133**, 12197-12219.
- S4.** P. A. Korevaar, C. Schaefer, T. F. A. de Greef and E. W. Meijer, *J. Am. Chem. Soc.*, 2012, **134**, 13482-13491.
- S5.** R. F. Goldstein, L. Stryer, *Biophys. J.*, 1986, **50**, 583-599.
- S6.** a) A. J. Markvoort, H. M. M. ten Eikelder, P. A. J. Hilbers, T. F. A. de Greef and E. W. Meijer, *Nat. Commun.*, 2011, **2**, 509; b) H. M. M. ten Eikelder, A. J. Markvoort, T. F. A. de Greef and P. A. J. Hilbers, *J. Phys. Chem. B*, 2012, **116**, 5291-5301.
- S7.** P. A. Heiney, *IUCR Commission on Powder Diffraction Newsletter*, 2005, **32**, 9-11.
- S8.** N. Godberg, A. Crispini, M. Ghedini, M. Carini, F. Chiaravalloti and A. Ferrise, *J. Appl. Cryst.*, 2014, **47**, 668-679.
- S9.** D. Sahoo, M. Peterca, E. Aqad, B. E. Partridge, P. A. Heiney, R. Graf, H. W. Spiess, X. Zeng and V. Percec, *J. Am. Chem. Soc.*, 2016, **138**, 14798-14807.
- S10.** M. Hecht, B. Soberats, J. Zhu, V. Stepanenko, S. Agarwal, A. Greiner and F. Würthner, *Nanoscale Horiz.*, 2019, **4**, 169-174.
- S11.** F. Neese, *WIREs Comput. Mol. Sci.*, 2012, **2**, 73-78.
- S12.** a) A. D. Becke, *J. Chem. Phys.*, 1993, **98**, 5648-5652; b) P. J. Stephens, F. J. Devlin, C. F. Chabalowski and M. J. Frisch, *J. Phys. Chem.*, 1994, **98**, 11623-11627.
- S13.** A. Schaefer, C. Huber and R. Ahlrichs, *J. Chem. Phys.*, 1994, **100**, 5829-5835.
- S14.** M. D. Hanwell, D. E. Curtis, D. C. Lonie, T. Vandermeersch, E. Zurek and G. R. Hutchison, *J. Cheminformatics*, 2012, **4**:17.
- S15.** C. Banhnwarth, S. Ehlert and S. Grimme, *J. Chem. Theory Comput.*, 2019, **15**, 1652-1671.
- S16.** O. Sumner Makin, P. Sikorski and L. C. Serpell, *J. Appl. Crystallogr.*, 2007, **40**, 966-972
- S17.** H. R. Rawls, M. A. El-Bayoumi and M. Kasha, *Pure Appl. Chem.*, 1965, **11**, 371-392.
- S18.** C. Würth, M. Grabolle, J. Pauli, M. Spieles, U. Resch-Genger, *Nat. Protoc.* 2013, **8**, 1535-1550.